AIAA JOURNAL
Vol. 48, No. 1, January 2010

# Finite Element Method Applied to Supersonic Flutter of Circular Cylindrical Shells

Farhad Sabri* and Aouni A. Lakis†
*École Polytechnique de Montréal, Montréal, Quebec H3T 1J4, Canada*

DOI: 10.2514/1.39580

**The method of analysis is a combination of Sander's thin shell theory and the classic finite element method, in which the nodal displacements are found from the exact solution of shell governing equations rather than approximated by polynomial functions. Piston theory with and without a correction factor for curvature is applied to derive aerodynamic damping and stiffness matrices. The influence of stress stiffness due to internal pressure and axial loading is also taken into account. Aeroelastic equations in hybrid finite element formulation are derived and solved numerically. Different boundary conditions of the shell, geometries, and flow parameters are investigated. In all study cases, the shell loses its stability due to coupled-mode flutter and a traveling wave is observed during this dynamic instability. The results are compared with existing experimental data and other analytical and finite element solutions. The present study shows efficient and reliable results that can be applied to the aeroelastic design and analysis of shells of revolution in aerospace vehicles.**

## Nomenclature

| | | |
|---|---|---|
| $[A]$ | = | coefficient matrix of shape functions; see Appendix B.1 |
| $a_\infty$ | = | freestream speed of sound |
| $[B]$ | = | coefficient matrix of strain vector; see Eq. (11) |
| $[C_f]$ | = | global aerodynamic damping matrix |
| $[c_f]$ | = | local aerodynamic damping matrix |
| $D$ | = | coefficient of elasticity matrix; see Eq. (6) |
| $E$ | = | Young's modulus |
| $\mathbf{F}_p$ | = | force vector due to the aerodynamic pressure field |
| $h$ | = | shell thickness |
| $i$ | = | complex number, $\sqrt{-1}$ |
| $K$ | = | bending stiffness of shell; see Eq. (6) |
| $[K]$ | = | global stiffness matrix for a shell |
| $[K_f]$ | = | global aerodynamic damping matrix |
| $[K_I]$ | = | global initial stiffness matrix for shell |
| $[k]$ | = | stiffness matrix for a shell element |
| $[k_f]$ | = | local aerodynamic stiffness matrix |
| $[k_I]$ | = | initial stiffness matrix for a shell element |
| $L$ | = | shell length |
| $l$ | = | element length |
| $M$ | = | Mach number |
| $[M_s]$ | = | global mass matrix for a shell |
| $M_x, M_\theta, M_{x\theta}$ | = | stress couples for a circular cylindrical shell |
| $[m]$ | = | mass matrix for a shell element |
| $[N]$ | = | shape functions; see Eq. (10) |
| $N_x, N_\theta, N_{x\theta}$ | = | stress resultant for a circular cylindrical shell |
| $\bar{N}_x, \bar{N}_\theta$ | = | stress resultant due to shell internal pressure and axial compression |
| $[P]$ | = | elasticity matrix |
| $P_a$ | = | aerodynamic pressure |
| $P_m, P_x$ | = | shell internal pressure and axial compression |
| $P_\infty$ | = | freestream static pressure |
| $[Q]$ | = | coefficient matrix of strain vector; see Appendix B.2 |
| $Q_x, Q_\theta$ | = | transverse stress resultant for a circular cylindrical shell |
| $R$ | = | shell radius |
| $[R]$ | = | coefficient matrix of shape functions; see Appendix B.1 |
| $[R_f]$ | = | coefficient matrix of aerodynamic pressure field; see Appendix B.3 |
| $r$ | = | radial coordinate |
| $\mathbf{r}$ | = | vector; see Eq. (18) |
| $[T]$ | = | coefficient matrix of shape functions; see Appendix B.1. |
| $T_{t,\infty}$ | = | stagnation temperature |
| $U$ | = | axial displacement |
| $U_i$ | = | potential energy due to initial strain |
| $U_\infty$ | = | freestream velocity |
| $u_n$ | = | component of $U$ associated with the $n$th circumferential wave number |
| $V$ | = | circumferential displacement |
| $\upsilon$ | = | Poisson's ratio |
| $v_n$ | = | component of $V$ associated with the $n$th circumferential wave number |
| $W$ | = | radial displacement |
| $w_n$ | = | component of $W$ associated with the $n$th circumferential wave number |
| $x$ | = | longitudinal coordinate |
| $\gamma$ | = | adiabatic exponent |
| $\delta_i, \delta_j$ | = | displacement at nodes $i$ and $j$ |
| $\boldsymbol{\epsilon}$ | = | strain vector |
| $\varepsilon_x, \varepsilon_\theta, \varepsilon_{x\theta}$ | = | axial, circumferential, and shear strains for a circular cylindrical shell |
| $\theta$ | = | circumferential coordinate |
| $\kappa_x, \kappa_\theta$ | = | bending strains for a circular cylindrical shell |
| $\kappa_{x\theta}$ | = | twisting strain for a circular cylindrical shell |
| $\lambda_j$ | = | complex roots of the characteristic equation; see Eqs. (4) |
| $\rho$ | = | shell density |
| $\rho_f$ | = | fluid density |
| $\boldsymbol{\sigma}$ | = | stress vector |
| $\varphi_{xx}, \varphi_{x\theta}, \varphi_n$ | = | elastic rotations for a circular cylindrical shell |
| $\omega$ | = | oscillation frequency |

Received 7 July 2008; revision received 24 July 2009; accepted for publication 16 September 2009. 

*Postdoctoral Fellow, Section of Applied Mechanics, Department of Mechanical Engineering; farhad.sabri@polymtl.ca. Member AIAA.

†Professor, Section of Applied Mechanics, Department of Mechanical Engineering, aouni.lakis@polymtl.ca

## I. Introduction

SHELLS and plates are key structures in aerospace vehicles. For example, these elements are frequently used in the fuselage and

engine nacelles of airplanes and the skin of space shuttles. As they are exposed to external airflow and particularly supersonic flow, dynamic instability and flutter become key considerations in the design and analysis of skin panels. Cylindrical shells can also show this kind of aeroelastic instability, and prevention of this behavior is one of the primary design criteria faced by aeronautical engineers.

After introducing the application of piston theory in the aeroelastic modeling presented by Ashley and Zartarian [1], a number of interesting experimental and theoretical studies [2–5] were conducted to investigate supersonic flutter of a cylindrical shell in the late 1960s. In general, all of this research was concerned with the development of an analytical relation to describe the effect of shell and flow parameters on the critical flutter frequency. Aeroelastic models were developed by applying the theory of shells (i.e., linear or nonlinear Donell shallow-shell theory) in conjunction with linear or nonlinear piston theory to account for fluid–structure interaction. The resulting governing equations were treated numerically using the Galerkin method. In most cases, the theory did not agree well with experimentally obtained results [6]. A comprehensive experimental test was done by Olson and Fung [2]. They examined the effects caused by shell boundary conditions and the initial strain state due to internal pressure and axial load. It was observed that a pressurized cylindrical shell fluttered at a lower level of freestream static pressure than predicted by theory [3]. Later, Evensen and Olson [4,5] presented a nonlinear analysis for calculating the limit cycle amplitude of a cylindrical shell using a four-mode approximation for the shell deflection. They observed a circumferentially traveling wave flutter similar to that occurring during the experimental study in [2]. Dowell [7] also investigated the behavior of a cylindrical shell in supersonic flow for different flow and shell parameters. An extensive description of panel flutter modeling has been reported in his book [8]. A study by Carter and Stearman [9] showed that agreement between the theory and experiments reported in the literature exists in cases that involve a small amount of static preload acting on the shell. In an effort to compensate for the disagreement of other cases, Barr and Stearman [10] presented an overall improvement in the correlation between theoretical analysis and experimental data by applying an initial imperfection and prestability deformation caused by static loading. In a follow-up study [11], they found that supersonic flow has no influence on the critical buckling load of a cylindrical shell while a small amount of axial load significantly decreases the flutter speed of the shell. Amabili and Pellicano [12] included geometric nonlinearities in their study, which modeled the supersonic flutter of a circular cylindrical shell. Based on the selection of expansion modes to discretize the aeroelastic equations to facilitate their solution, they succeeded in capturing the nonlinear behavior of the shell correctly. Amabili and Pellicano [13] also applied the nonlinear piston theory with a shell imperfection to reproduce the experimental data for a pressurized cylindrical shell. In this case, results show that the nonlinear piston theory has no influence on the onset of flutter but knowledge of axisymmetric imperfections can help to predict it correctly.

There are also some researchers who focused on the numerical solution of this problem. They developed their solutions using a variational formulation. For example, the equations of virtual displacements were solved using the finite element method (FEM). Aeroelastic governing equations were derived by applying classical shell theory based on the Kirchhoff–Love hypothesis coupled with the piston theory for evaluation of aerodynamic forces. For example, Bismarck-Nasr [14] developed a FEM applied to supersonic flutter of a circular shell subjected to internal pressure and axial loading. The numerical results were compared with experimental and analytical solutions. Ganapathi et al. [15] modeled an orthotropic and laminated anisotropic circular cylindrical shell in supersonic flow using FEM and did a parametric study to see the effect of different shell geometries on the flutter boundaries. For more details, interested readers can refer to the review paper presented by Bismarck-Nasr [16].

For such a problem, which contains complex structures, boundary conditions, materials, and loading, an analytical model becomes very complicated to go through variation of all factors affecting the flutter boundaries; therefore, numerical methods like FEM are considered a powerful method for such an analysis. The first objective of the study presented in this article was to adequately describe supersonic flutter of a circular cylindrical shell and present a numerical model of existing experimental data. The second objective was to determine an efficient choice of shell theory for developing a finite element model. Most of the published papers in the literature have applied general linear or nonlinear shell theory based on the Kirchhoff–Love hypothesis. These developments can only be applied to thin and uniform shells. In cases of multilayered shells or shells of nonuniform thickness (i.e., allowing for axial variation in thickness), difficulties occur during the calculation of panel flutter. This study is focused on the development of a circumferential hybrid element for a circular cylindrical shell in supersonic flow. The procedure is similar to the finite element development done for circular cylindrical shell by Lakis and Paidoussis [17] and also Sabri and Lakis [18]. These developments resulted in precise and fast convergence with few numerical difficulties. The accuracy of this method is well established because the elastic displacement functions are derived directly from the shell governing equations rather than approximated by polynomial functions. The element is a cylindrical frustum instead of the usual rectangular shell element. The linear Sander's shell theory, in which all the strains vanish for rigid-body motions but the other theories are incapable of this attribute, is coupled with the linearized first-order piston theory [1] including the curvature correction term [19] to take into account fluid–structure interaction. Initial stress stiffening in the presence of shell internal pressure and axial compression is also applied in the formulation. Many researchers tackle this problem analytically or numerically with lots of effort, whereas this proposed method can be applied in a reliable way without any computational cost and effort, particularly during the preliminary stage of design during which different boundary conditions and configurations have to be tested to find the optimum design. The linear theory developed here is adequate to predict the onset of flutter; however, nonlinear shell theory required to capture the actual limit cycle amplitudes of flutter is left for future study.

## II. Structural Modeling

### A. Hybrid Element

Sander's shell theory [20] is based on Love's first approximation, in which the inconsistency related to the fact that strains for small rigid-body rotations of the shell do not vanish has been removed. Using a cylindrical coordinate system, the equilibrium equations for a cylindrical shell according to this theory [20] are

$$\frac{\partial N_x}{\partial x}+\frac{1}{R}\frac{\partial N_{x\theta}}{\partial \theta}-\frac{1}{2R^2}\frac{\partial M_{x\theta}}{\partial \theta}=0$$

$$\frac{\partial N_{x\theta}}{\partial x}+\frac{1}{R}\frac{\partial N_{\theta}}{\partial \theta}+\frac{1}{2R}\frac{\partial M_{x\theta}}{\partial x}+\frac{1}{R}Q_{\theta}=0$$

$$\frac{\partial Q_x}{\partial x}+\frac{1}{R}\frac{\partial Q_{\theta}}{\partial \theta}-\frac{1}{R}N_{\theta}=0 \qquad \frac{\partial M_x}{\partial x}+\frac{1}{R}\frac{\partial M_{x\theta}}{\partial \theta}-Q_x=0$$

$$\frac{\partial M_{x\theta}}{\partial x}+\frac{1}{R}\frac{\partial M_{\theta}}{\partial \theta}-Q_{\theta}=0 \tag{1}$$

where $R$ is the mean shell radius; $N_x$ and $N_\theta$ are the normal stress resultants in axial and circumferential directions, respectively; and $N_{x\theta}$ represents the shear stress resultant in the $x\theta$ plane. $M_x$ and $M_\theta$ are the stress couples in the axial and circumferential directions, respectively, and $M_{x\theta}$ is the couple in the $x\theta$ plane. In Eq. (1), $Q_x$ is the transverse stress resultant in the axial direction and $Q_\theta$ represents the transverse stress resultant in the circumferential direction. The strain-displacement equations for three infinitesimal displacements in the axial $U$, radial $W$, and circumferential $V$ directions are [20]

$$\begin{Bmatrix} \varepsilon_x \\ \varepsilon_\theta \\ \varepsilon_{x\theta} \\ \kappa_x \\ \kappa_\theta \\ \kappa_{x\theta} \end{Bmatrix} = \begin{Bmatrix} \frac{\partial U}{\partial x} \\ \frac{1}{R}\frac{\partial V}{\partial \theta}+\frac{W}{R} \\ \frac{1}{2}\left(\frac{\partial V}{\partial x}+\frac{1}{R}\frac{\partial U}{\partial \theta}\right) \\ -\frac{\partial^2 W}{\partial x^2} \\ -\frac{1}{R^2}\frac{\partial^2 W}{\partial \theta^2}+\frac{1}{R^2}\frac{\partial V}{\partial \theta} \\ -\frac{1}{R}\frac{\partial^2 W}{\partial \theta \partial x}+\frac{3}{4R}\frac{\partial V}{\partial x}-\frac{1}{4R^2}\frac{\partial U}{\partial \theta} \end{Bmatrix} \tag{2}$$

In Eq. (2), $\varepsilon_x$ and $\varepsilon_\theta$ are the strains in the axial and circumferential directions, respectively, and $\varepsilon_{x\theta}$ represents the strain in the $x\theta$ plane. $\kappa_x$ and $\kappa_\theta$ are the axial and circumferential strains, respectively, and $\kappa_{x\theta}$ is the twisting strain for a circular cylindrical shell.

The stress-strain relations for anisotropic shells are given by

$$\boldsymbol{\sigma} = [P]\boldsymbol{\epsilon} \tag{3}$$

where $[P]$ is the elasticity matrix for an anisotropic shell [21]. Upon substitution of Eqs. (2) and (3) into Eq. (1), a system of equilibrium equations can be obtained as a function of displacements:

$$L_J(U, W, V, P_{ij}) = 0 \tag{4}$$

where $L_J$ ($J = 1, 2, 3$) are three linear partial differential equations presented in Appendix A, and $P_{ij}$ are elements of the elasticity matrix that, for an isotropic shell, are given by

$$[p] = \begin{bmatrix} D & \upsilon D & 0 & 0 & 0 & 0 \\ \upsilon D & D & 0 & 0 & 0 & 0 \\ 0 & 0 & \frac{D(1-\upsilon)}{2} & 0 & 0 & 0 \\ 0 & 0 & 0 & K & \upsilon K & 0 \\ 0 & 0 & 0 & \upsilon K & K & 0 \\ 0 & 0 & 0 & 0 & 0 & \frac{K(1-\upsilon)}{2} \end{bmatrix} \tag{5}$$

where

$$K = \frac{Eh^3}{12(1-\upsilon^2)} \qquad D = \frac{Eh}{1-\upsilon^2} \tag{6}$$

and $E$ is Young's modulus, $\upsilon$ is Poisson's ratio, and $h$ is the shell thickness.

A circumferential cylindrical frustum based on the development done in [17,18] is applied to generate the mass and stiffness matrices of the structural model. This element type (see Fig. 1) has two nodal circles with two nodal points: $i$ and $j$. There are 4 degrees of freedom at each node: axial, radial, circumferential displacement, and rotation. This kind of element makes it possible to use thin shell equations easily to find the exact solution of displacement functions rather than an approximation with polynomial functions, as is done in classic FEM. This element selection results in a hybrid element for which the convergence criterion of the finite element method is provided with greater accuracy. Considering the displacement in the normal manner as

$$U(r, x, \theta) = \sum_n u_n(x)\cos(n\theta) \qquad W(r, x, \theta) = \sum_n w_n(x)\cos(n\theta)$$
$$V(r, x, \theta) = \sum_n v_n(x)\sin(n\theta) \tag{7}$$

where $n$ is the circumferential wave number, Lakis and Paidoussis [17] found the exact analytical solution for displacements based on the characteristic equation associated with a system of Eqs. (4). The final form of the displacement functions was obtained as

$$\begin{Bmatrix} U(x, r, \theta) \\ W(x, r, \theta) \\ V(x, r, \theta) \end{Bmatrix} = [N]\begin{Bmatrix} \delta_i \\ \delta_j \end{Bmatrix} \tag{8}$$

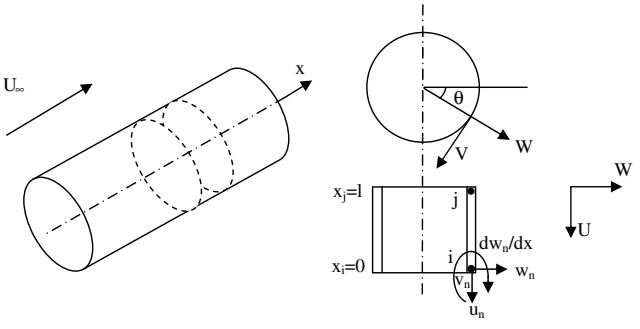


**Fig. 1 Geometry of cylindrical frustum element.**

where the nodal displacement vector $\{\delta\}$ and matrix $[N]$ are defined by

$$\{\delta_i\} = \begin{Bmatrix} u_{ni} \\ w_{ni} \\ (\mathrm{d}w_n/\mathrm{d}x)_i \\ v_{ni} \end{Bmatrix} \tag{9}$$

$$[N] = [T][R][A]^{-1} \tag{10}$$

In Eq. (10), the matrices $[T]$, $[R]$, and $[A]$ are shown in Appendix B.1. By introducing Eq. (8) into Eq. (2) the strain vector can be found:

$$\boldsymbol{\epsilon} = \begin{bmatrix} [T] & [0] \\ [0] & [T] \end{bmatrix}[Q][A^{-1}]\begin{Bmatrix} \delta_i \\ \delta_j \end{Bmatrix} = [B]\begin{Bmatrix} \delta_i \\ \delta_j \end{Bmatrix} \tag{11}$$

where matrix $[Q]$ is given in Appendix B.2. Now the stress resultant is found from Eqs. (11) and (3):

$$\boldsymbol{\sigma} = [P][B]\begin{Bmatrix} \delta_i \\ \delta_j \end{Bmatrix} \tag{12}$$

Therefore, the mass and stiffness matrices for each element are derived [22]:

$$[m] = \rho h \iint [N]^T[N]\,\mathrm{d}A \qquad [k] = \iint [B]^T[P][B]\,\mathrm{d}A \tag{13}$$

where $\rho$ is the shell density and $\mathrm{d}A = r\mathrm{d}x\mathrm{d}\theta$. For the entire shell geometry, the standard assembly technique in FEM can be used along with the application of the appropriate boundary conditions to find the global mass and stiffness matrices. Further information regarding the derivation of the stiffness and mass matrix equations for this combined finite element analysis with classic thin shell theory can be found in [17].

### B. Initial Stress Stiffness

The influence of membrane forces on the dynamic stability of a cylindrical shell in the presence of supersonic airflow is investigated here. These membrane forces are due to pressure differential across the shell $P_m$ and axial compression $P_x$. It is assumed that the shell is in an equilibrium condition and also has not reached its buckling state. The initial in-plane shear, static bending, and transverse shear are also ignored for this analysis. The stress resultants due to internal pressure $P_m$ and axial compression $P_x$ are

$$\bar{N}_x = -\frac{P_x}{2\pi R} \qquad \bar{N}_\theta = P_m R \tag{14}$$

The potential energy due to this initial strain is equal to [23]

$$U_i = 1/2\int_0^l \int_0^{2\pi} [\bar{N}_x\varphi_{\theta\theta}^2 + \bar{N}_\theta\varphi_{xx}^2 + (\bar{N}_x + \bar{N}_\theta)\varphi_n^2]R\;\mathrm{d}\theta\,\mathrm{d}x \tag{15}$$

where $l$ is the element length, $\varphi_{xx}$ is the strain rotation about the $x$ axis, $\varphi_{\theta\theta}$ is about the normal to the $x\theta$ plane, and $\varphi_n$ is the rotation about the normal to the shell element. This rotation vector is given by [20]

$$\varphi_{\theta\theta} = -\frac{\partial W}{\partial x} \qquad \varphi_{xx} = \frac{1}{R}\left(V - \frac{\partial W}{\partial \theta}\right)$$
$$\varphi_n = \frac{1}{2}\left(-\frac{1}{R}\frac{\partial U}{\partial \theta} + \frac{\partial V}{\partial x}\right) \tag{16}$$

If the displacements are replaced by Eq. (8), the potential energy in terms of nodal degrees of freedom is generated:

$$U_i = 1/2\int_0^l \int_0^{2\pi} \mathbf{r}^T \begin{bmatrix} \bar{N}_x & 0 & 0 \\ 0 & \bar{N}_\theta & 0 \\ 0 & 0 & \bar{N}_x + \bar{N}_\theta \end{bmatrix}\mathbf{r}R\,\mathrm{d}\theta\,\mathrm{d}x \tag{17}$$

where vector $\mathbf{r}$ is defined as

$$\mathbf{r} = \begin{bmatrix} 0 & -\frac{\partial}{\partial x} & 0 \\ 0 & -\frac{1}{R}\frac{\partial}{\partial \theta} & 0 \\ -\frac{1}{2R}\frac{\partial}{\partial \theta} & 0 & \frac{1}{2}\frac{\partial}{\partial x} \end{bmatrix} \begin{Bmatrix} U \\ W \\ V \end{Bmatrix} = [C_0][N] \begin{Bmatrix} \delta_i \\ \delta_j \end{Bmatrix} \tag{18}$$

The initial stiffness matrix for each element becomes

$$[k_l] = \int_0^l \int_0^{2\pi} [N]^T [C_0]^T \begin{bmatrix} \bar{N}_x & 0 & 0 \\ 0 & \bar{N}_\theta & 0 \\ 0 & 0 & \bar{N}_x + \bar{N}_\theta \end{bmatrix} [C_0]^T [N]^T R \, \mathrm{d}\theta \, \mathrm{d}x \tag{19}$$

With the help of Maple software, analytical integration of Eq. (19) for each element is done. After assembling the whole initial stiffness matrix, it is added to the global stiffness matrix calculated in Eq. (13).

## III. Aerodynamic Modeling

Piston theory is a powerful tool for aerodynamic modeling in aeroelasticity. For a cylinder subjected to an external supersonic airflow parallel to the centerline of the shell, the fluid–structure effect due to external pressure loading can be taken into account using linearized first-order potential theory [8] with (or without) the curvature correction term [19]:

$$P_a = \frac{\gamma p_\infty M^2}{(M^2-1)^{1/2}} \left[ \frac{\partial W}{\partial x} + \frac{M^2-2}{M^2-1} \frac{1}{U_\infty} \frac{\partial W}{\partial t} - \frac{W}{2R(M^2-1)^{1/2}} \right] \tag{20}$$

where $P_\infty$, $U_\infty$, $M$, and $\gamma$ are the freestream static pressure, freestream velocity, Mach number, and adiabatic exponent of air, respectively. For sufficiently high Mach number ($M \geq 2$) and neglecting the curvature term $\frac{W}{2R(M^2-1)^{1/2}}$, this equation is simplified to the so-called linear piston theory [1]:

$$P_a = -\gamma P_\infty \left[ M \frac{\partial W}{\partial x} + \frac{1}{a_\infty} \frac{\partial W}{\partial t} \right] \tag{21}$$

where $a_\infty$ is the freestream speed of sound.

The radial displacement can be developed based on an analytical solution [18] in terms of $\lambda_j$, the complex roots of a characteristic equation related to Eq. (4), and the oscillation frequency of the shell, $\omega$. It can be written as

$$W = \sum_{j=1}^{8} e^{i(\lambda_j \frac{x}{R} + \omega t)} \cos(n\theta) = \sum_{j=1}^{8} W_j \tag{22}$$

In Sec. III.A, the pressure field for each aerodynamic loading model is expressed in terms of nodal displacements.

### A. Piston Theory

The pressure field expressed by Eq. (21) can be rewritten as

$$P_a = -\gamma P_\infty \sum_{j=1}^{8} \left( \frac{1}{a_\infty} \frac{\partial W_j}{\partial t} + M \frac{\partial W_j}{\partial x} \right) \tag{23}$$

Introducing Eqs. (8) and (22) into Eq. (23), the aerodynamic pressure may be defined:

$$\{P_a\} = \begin{Bmatrix} 0 \\ p_{\text{radial}} \\ 0 \end{Bmatrix} = -\gamma \frac{P_\infty}{a_\infty} [T][R_f][A^{-1}] \begin{Bmatrix} \dot{\delta}_i \\ \dot{\delta}_j \end{Bmatrix} - \left( i \frac{\lambda_j}{R} \right) \gamma P_\infty M [T][R_f][A^{-1}] \begin{Bmatrix} \delta_i \\ \delta_j \end{Bmatrix} \tag{24}$$

where elements of matrix $[R_f]$ are shown in Appendix B.3.

### B. Piston Theory with the Curvature Term

Equation (20) includes the curvature term and can be used to describe the aerodynamic pressure field as follows:

$$\{P_a\} = \begin{Bmatrix} 0 \\ p_{\text{radial}} \\ 0 \end{Bmatrix} = \frac{-\rho_\infty U_\infty^2}{(M^2-1)^{1/2}} \frac{1}{U_\infty} \left( \frac{M^2-2}{M^2-1} \right) [T][R_f][A^{-1}] \begin{Bmatrix} \dot{\delta}_i \\ \dot{\delta}_j \end{Bmatrix} + \left( i \frac{\lambda_j}{R} \right) \frac{-\rho_\infty U_\infty^2}{(M^2-1)^{1/2}} [T][R_f][A^{-1}] \begin{Bmatrix} \delta_i \\ \delta_j \end{Bmatrix} - \frac{-\rho_\infty U_\infty^2}{(M^2-1)^{1/2}} \left( \frac{1}{2(M^2-1)^{1/2}R} \right) [T][R_f][A^{-1}] \begin{Bmatrix} \delta_i \\ \delta_j \end{Bmatrix} \tag{25}$$

where $\rho_\infty$ is the freestream air density. It is seen that the freestream static pressure and velocity can be linked using the following equations:

$$U_\infty = M \cdot a_\infty \tag{26}$$

$$a_\infty = \sqrt{\gamma \frac{p_\infty}{\rho_\infty}} \tag{27}$$

### C. Aerodynamic Damping and Stiffness

The general force vector due to the pressure field is written as:

$$\mathbf{F}_p = \iint [N]^T \{p_a\} \, \mathrm{d}A \tag{28}$$

For example, using the piston theory to account for pressure loading, Eqs. (10) and (24) can be substituted into Eq. (28) and the aerodynamic damping, $[c_f]$, and stiffness, $[k_f]$, for each element can be found:

$$[c_f] = [A^{-1}]^T [D_f][A^{-1}] \qquad [k_f] = [A^{-1}]^T [G_f][A^{-1}] \tag{29}$$

where

$$[D_f] = -\frac{\gamma}{a_\infty} P_\infty \pi r \int_0^l [R]^T [R_f] \, \mathrm{d}x$$
$$[G_f] = -i \frac{\lambda_j}{r} \gamma P_\infty M \pi r \int_0^l [R]^T [R_f] \, \mathrm{d}x \tag{30}$$

The same procedures can be done to derive the local damping and stiffness matrices by inserting the different pressure fields mentioned

**Table 1 Convergence test for shell case I**

| No. of elements | $\omega_1$, Hz | $\omega_2$, Hz | $\omega_3$, Hz | $\omega_4$, Hz | $P_\infty$, Pa | $n_{\text{critical}}$ |
|---|---|---|---|---|---|---|
| 6 | 318.836 | 320.253 | 333.286 | 367.256 | 689 | 26 |
| 8 | 303.339 | 307.551 | 323.062 | 357.826 | 2296 | 26 |
| 10 | 297.195 | 302.330 | 318.605 | 353.346 | 2930 | 26 |
| 13 | 293.237 | 298.898 | 315.574 | 350.165 | 3316 | 26 |
| 15 | 291.922 | 297.747 | 314.549 | 349.079 | 3440 | 26 |
| 16 | 291.455 | 297.343 | 314.204 | 348.744 | 3488 | 26 |
| 19 | 268.218 | 275.048 | 294.877 | 335.063 | 3578 | 25 |
| 20 | 268.047 | 274.899 | 294.742 | 334.912 | 3592 | 25 |

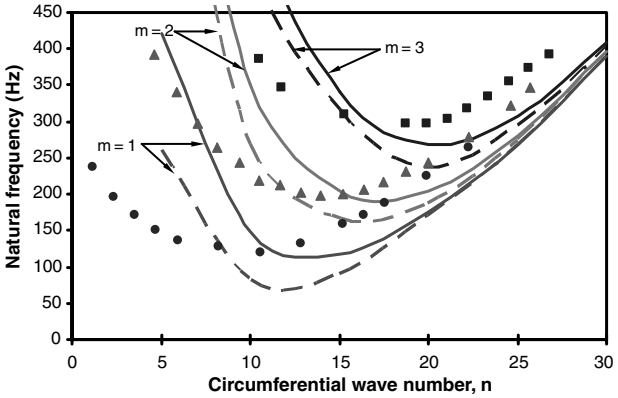


**Fig. 2 Natural frequencies of unstressed shell: a) case I: — simply supported ends, —— freely simply supported ends; and b) experiment: ● $m = 1$, ▲ $m = 2$, and ■ $m = 3$.**

in Sec. III.B into Eq. (28). Finally, global aerodynamic damping $[C_f]$ and aerodynamic stiffness $[K_f]$ matrices are found using the assembling procedure.

## IV. Aeroelastic Model in Finite Element Method

The governing equation of motion in a global system for a cylindrical shell exposed to an external supersonic flow is

$$[M_s]\{\ddot{\delta}\} - [C_f]\{\dot{\delta}\} + [[K_s] + [K_I] - [K_f]]\{\delta\} = 0 \qquad (31)$$

where the subscripts $s$ and $f$ refer to a shell in vacuo and fluid, respectively, and $I$ refers to a shell under axial compression and/or pressurized. To find the aeroelastic behavior of a shell, eigenvalues and eigenvectors of Eq. (31) are found by means of the equation reduction method. Equation (31) is therefore rewritten as

$$\begin{bmatrix} [0] & \frac{1}{\omega_0}[M_s] \\ \frac{1}{\omega_0^2}[M_s] & \frac{1}{\omega_0}[C_f] \end{bmatrix} \begin{Bmatrix} \ddot{\delta} \\ \dot{\delta} \end{Bmatrix} + \begin{bmatrix} -\frac{1}{\omega_0}[M_s] & [0] \\ [0] & [K] \end{bmatrix} \begin{Bmatrix} \dot{\delta} \\ \delta \end{Bmatrix} = 0 \qquad (32)$$

where $\omega_0$ is the first element of the elasticity matrix in Eq. (5) and the total stiffness matrix is

$$[K] = [K_s] + [K_I] - [K_f] \qquad (33)$$

The corresponding eigenvalue problem is given by

$$\left| [DD] - \frac{1}{\omega_0 \Lambda}[I] \right| = 0 \qquad (34)$$

where $[I]$ is the identity matrix, $\Lambda$ is the eigenvalue (complex frequency of the system), and $[DD]$ is

$$[DD] = \begin{bmatrix} [0] & [I] \\ \frac{1}{\omega_0^2}[K^{-1}][M_s] & -\frac{1}{\omega_0}[K^{-1}][C_f] \end{bmatrix} \qquad (35)$$

Matrices $[M_s]$, $[C_f]$, and $[K]$ are square matrices of order NDF$(N + 1)$, where NDF is the number of degrees of freedom at each node and $N$ is the number of elements used to discretize the shell geometry. Dynamic stability of the shell is investigated by studying the eigenvalues in the complex plane. The flutter onset occurs when the imaginary part of the eigenvalue changes from positive to negative.

**Table 2 Comparison of shell flutter boundary at $M = 3$ and $p_x = p_m = 0$**

| | $P_\infty$, Pa | $n_{\text{critical}}$ | $L$, m | $\upsilon$ | $E$, Pa |
|---|---|---|---|---|---|
| Experimental results [2] | 2620–2896 | 20 | 0.381 | 0.35 | $11 \times 10^{10}$ |
| Analytical results [9] | 2896 | 24 | 0.406 | 0.33 | $8.9 \times 10^{10}$ |
| Analytical results [3] | 3792 | 25 | 0.381 | 0.35 | $11 \times 10^{10}$ |
| Analytical results [12] | 2275 | 27 | 0.381 | 0.35 | $11 \times 10^{10}$ |
| FEM results [14] | 3875 | 34 | 0.406 | 0.33 | $8.9 \times 10^{10}$ |
| FEM results [15] | 3875 | 25 | 0.406 | 0.33 | $8.9 \times 10^{10}$ |
| FEM results [15] | 3875 | 26 | 0.381 | 0.35 | $11 \times 10^{10}$ |
| Present results | 3599 | 26 | 0.381 | 0.35 | $11 \times 10^{10}$ |
| Present results | 2633 | 25 | 0.406 | 0.33 | $8.9 \times 10^{10}$ |

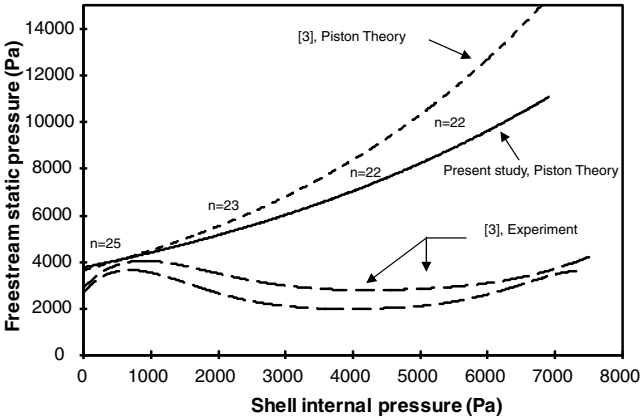


**Fig. 3 Cylindrical shell flutter boundaries.**

## V. Numerical Results and Discussion

In this section, numerical results are compared with existing experimental data and the analytical and numerical solutions. In all of

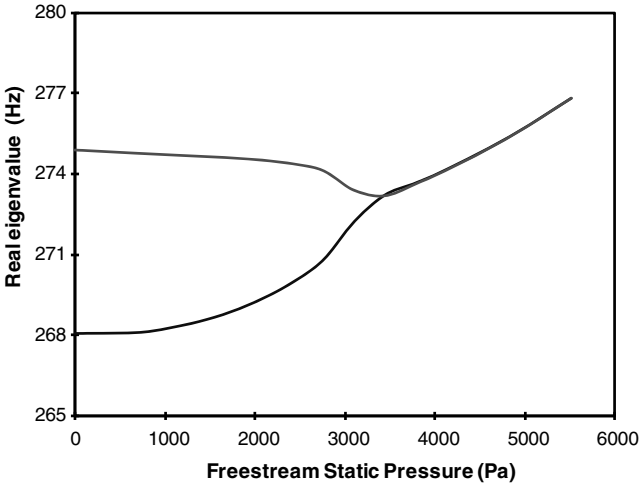


**a)**

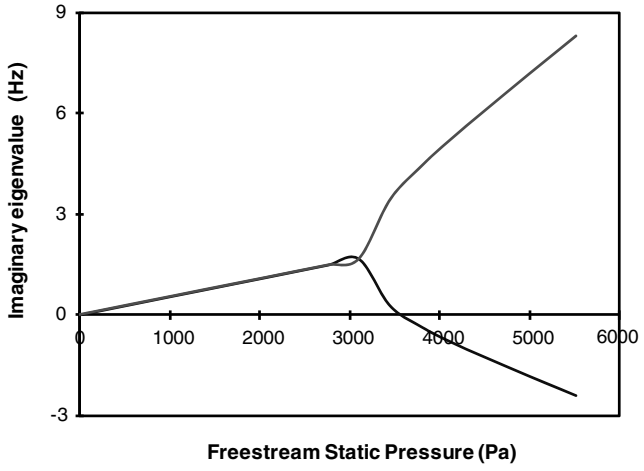


**b)**

**Fig. 4 Eigenvalues of system vs freestream static pressure, shell case I: a) real part, and b) imaginary part. Aerodynamic pressure evaluated by Eq. (20), $n = 25$, $P_m = 0.0$ Pa, $P_x = 0.0$ N.**

these studies, shell geometry and flow parameters have the following similar features: $E = 16 \times 10^6$ lb/in. ($11 \times 10^{10}$ N/m$^2$), $\upsilon = 0.35$, $h = 0.0040$ in. (0.0001015 m), $L = 15.4$ in. (0.381 m), $R =$ 8.00 in. (0.203 m), $\rho = 0.000833$ lb $\cdot$ s$^2$/in.$^4$ (8900 kg/m$^3$), $M =$ 3.00, $a_\infty = 8400$ in./s (213 m/s), and $T_{t\infty} = 120$°F (48.90°C), where $T_{t\infty}$ is the freestream stagnation temperature. This set of data was taken from the experiments done by Olson and Fung [2,3] in the NASA Ames Research Center (here referred to as case I). It is necessary to mention that in some of references different values for $L = 16$ in. (0.406 m), $E = 13 \times 10^6$ lb/in.$^2$ ($8.9 \times 10^{10}$ Pa), and $\upsilon = 0.33$ have been reported (referred to as case II). As a consequence, in the present analysis a comparison of numerical results was sought for each given set of data.

### A. Convergence Test

In finite element analysis, the number of elements has a significant influence on the final results. Therefore, a set of calculations (for case I) was done to find the appropriate number of elements for shell discretizing. As shown in Table 1, convergence of the natural frequency using 20 elements is sufficient for further analysis.

### B. Boundary Condition

For the test case in [3], the shell tested in a supersonic wind tunnel had complex boundary conditions. To obtain reliable numerical results, two different boundary conditions were applied to find the effective ends. The numerical prediction of natural frequencies is shown in Fig. 2 along with the experimental data of Olson and Fung [2]. For low values of circumferential mode number, $n$, the free simply supported boundary ($V = W = 0$) lies between the experimental and simply supported ends ($V = W = U = 0$). For high values of $n$, these two conditions approach each other and the experimental results lie above both of them. This discrepancy has been reported because of errors during measurement of the shell thickness [2]. It seems that the free simply supported case offers a good approximation to present effective ends of the shell during the flutter calculation, particularly for large values of the circumferential wave number.

### C. Validation

For both sets of data (cases I and II), numerical results of this study compared to the experimental, theoretical, and numerical analyses are presented in Table 2. In all of the cases, instability occurred in the form of coupled-mode flutter. The proposed FEM shows very good agreement with experimental and analytical results and also has better capabilities for aeroelastic stability prediction in terms of critical $p_\infty$ and $n$ compared to the other FEM methods. In Fig. 3, the results of flutter boundary for the pressurized shell have been presented and compared with the analytical experimental data of [3]. It can be seen that both studies predict a larger stabilizing effect of the moderate shell internal pressure than the experiments.

### D. Effect of the Curvature Term of Piston Theory

Figure 4 shows some typical complex frequencies versus freestream static pressure, $P_\infty$, for $n = 25$. Only the first and second axial modes are shown ($m = 1,\ 2$). Aerodynamic pressure is evaluated using Eq. (20). In Fig. 4a, the real part of the complex

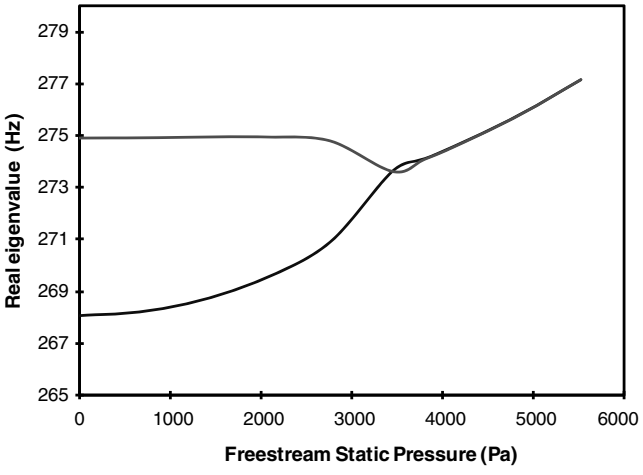


a)

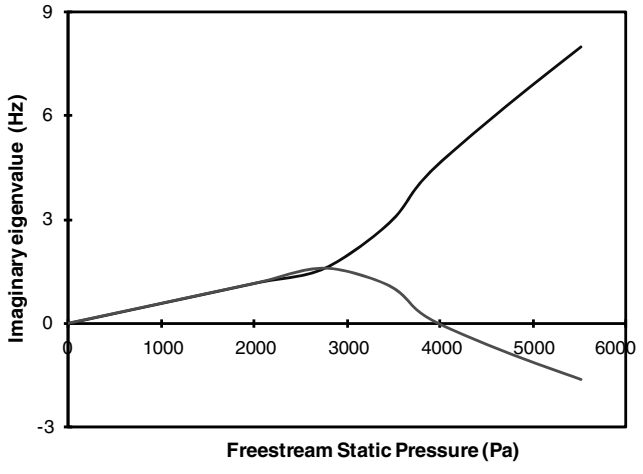


b)

**Fig. 5 Eigenvalues of system vs freestream static pressure, shell case I: a) real part, and b) imaginary part. Aerodynamic pressure evaluated by Eq. (21), $n = 25$, $P_m = 0.0$ Pa, $P_x = 0.0$ N.**

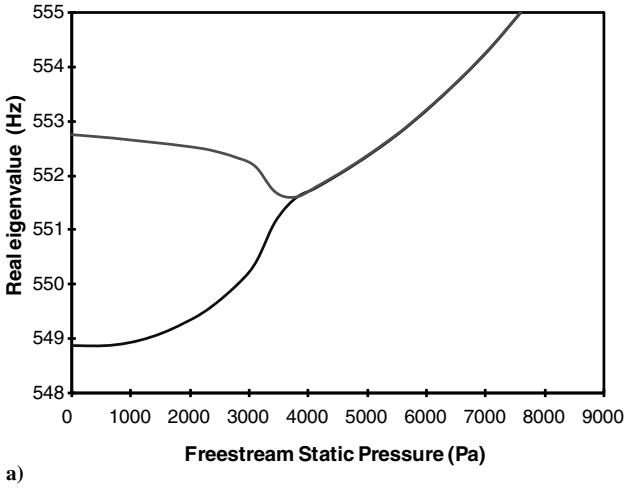


a)

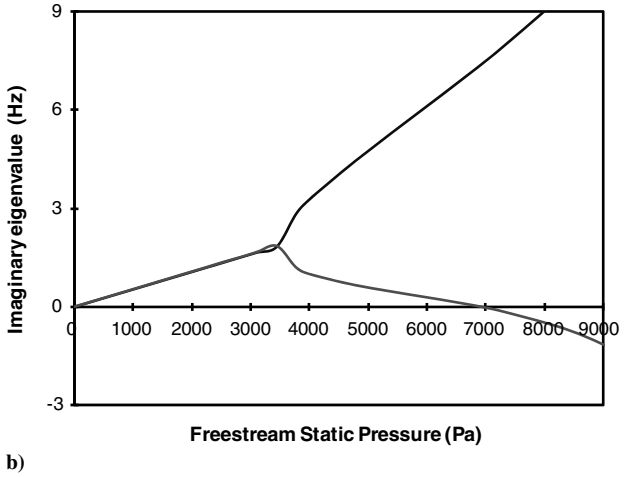


b)

**Fig. 6 Eigenvalues of system vs freestream static pressure, shell case I: a) real part, and b) imaginary part. Aerodynamic pressure evaluated by Eq. (20), $n = 23$, $P_m = 3447$ Pa, $P_x = 0.0$ N.**

frequency for the first mode increases whereas, for the second mode, it decreases as $P_\infty$ increases. For higher values of $P_\infty$ these real parts eventually merge into a single mode. If $P_\infty$ is increased still further, the shell loses stability at $P_\infty = 3592$ Pa. This instability is due to coupled-mode flutter because the imaginary part of the complex frequency (which represents the damping of the system) crosses the zero value (see Fig. 4b) and makes the vibration amplitude grow. Figure 5 presents the complex frequencies of the aerodynamic pressure if Eq. (21) is used for the calculation. The real and imaginary parts of the first and second modes show the same behavior as the freestream static pressure increases, but the onset of flutter is at $P_\infty = 4136$ Pa. Prediction of the critical freestream static pressure using Eq. (20) provides a closer match to experimental results than evaluating the pressure field using Eq. (21). As expected, the piston theory with the correction term to account for shell curvature produces a better approximation for the pressure loading acting on a curved shell exposed to supersonic flow.

### E. Effect of Initial Strain and Aspect Ratio

To investigate the effect of shell internal pressure, complex frequencies for the critical circumferential wave number $n = 23$ with shell internal pressure $P_m = 3447$ Pa were calculated and are shown in Fig. 6. In this case the critical freestream static pressure is $P_\infty = 6894$ Pa; due to the increase in stiffness of the shell because of applied internal pressure, flutter onset occurred at a higher value of $P_\infty$. In Fig. 7, the flutter boundary for the shell geometry of case II under different internal pressures is shown. The lowest critical value of freestream static pressure for each circumferential wave number

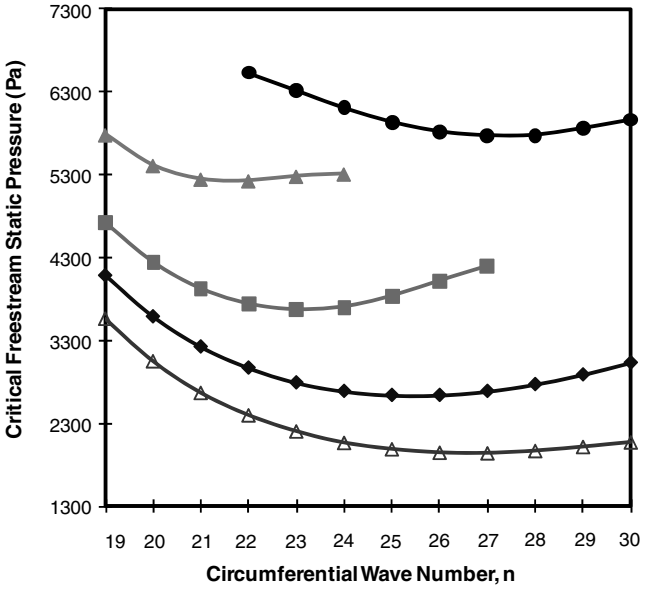


**Fig. 7 Flutter boundaries for stressed shell, shell case I, $P_x = 0.0$ N: ◆ $P_m = 0.0$ Pa, ■ $P_m = 1696$ Pa, ▲ $P_m = 3447$ Pa, ● $P_m = 4826Pa$, △ $P_x = 133.5$ N, $P_m = 0.0$ Pa.**

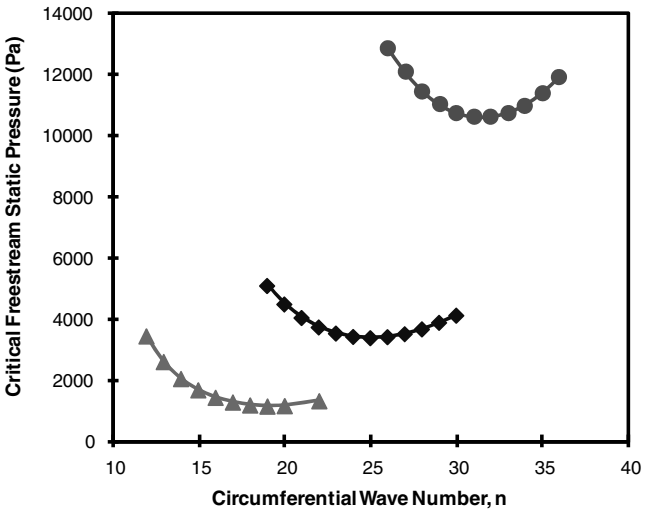


**Fig. 8 Flutter boundaries for different $L/R$ ratio, shell case I, $P_m = 0.0$ Pa, $P_x = 0.0$ N: ▲ $L/R = 4$, ◆ $L/R = 2$, ● $L/R = 1$.**

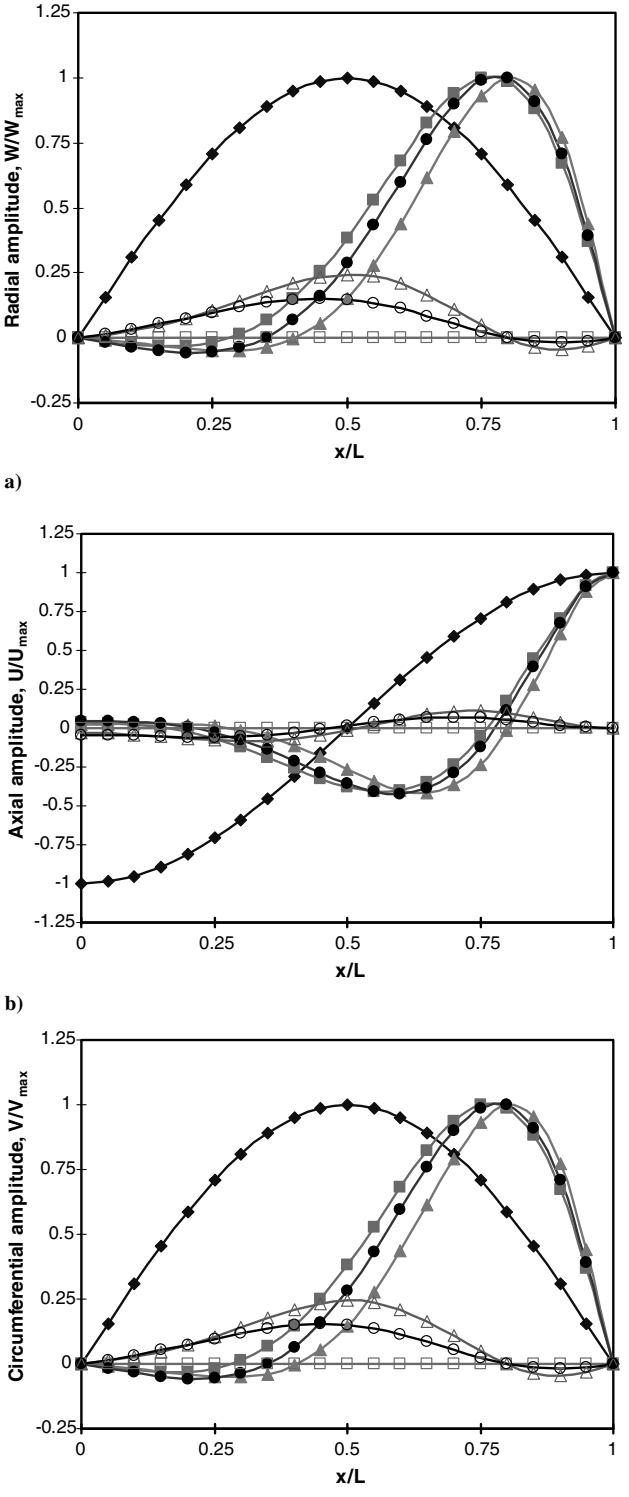


**Fig. 9 Mode shape variation with freestream static pressure, shell case I, $n = 25$, $m = 1$: a) radial, b) axial, and c) circumferential. ◆ free vibration $P_\infty = 0.0$ Pa, ■ cosine mode $P_\infty = 3102$ Pa, □ sine mode $P_\infty = 3102$ Pa, ● cosine mode $P_\infty = P_{\text{critical}} = 3592$ Pa, ○ sine mode $P_\infty = P_{\text{critical}} = 3592$ Pa, ▲ cosine mode $P_\infty = 5170$ Pa, △ sine mode $P_\infty = 5170$ Pa.**

**Table 3 Critical freestream static pressure for different shell boundary conditions, $P_x = P_m = 0$**

| Case I | $P_\infty$, Pa | $n_{\text{critical}}$ | Coupled mode |
|---|---|---|---|
| Free simply supported at one end, free at the other end | 2668 | 25 | 1–2 |
| Free simply supported at both ends | 3592 | 25 | 1–2 |
| Free at both ends | 3545 | 25 | 2–3 |
| Clamped at both ends | 4791 | 25 | 1–2 |

becomes larger when $P_m$ is increased. It is observed that shell internal pressure has a stabilizing influence. Note that experiments [2] demonstrated that for moderate values of $P_m$ the shell loses it dynamic stability up to an even unpressurized level whereas small and high values of $P_m$ stabilize the shell completely. This behavior is explained quite well by considering shell imperfections during the analysis [9,13]. The effect of axial compression on the flutter boundary is also shown in Fig. 7. The axial load $P_x$ decreases the stiffness of the shell, which results in a lower critical freestream static pressure than an unstressed shell. Figure 8 shows the case of different $L/R$ ratios. The critical freestream static pressure for a lower ratio of $L/R$ increases rapidly and the critical circumferential wave number also increases. For $L/R = 4$ the shell loses it stability at $n = 18$ and $P_\infty = 1179$ Pa, whereas for $L/R = 1$ the onset of flutter is at $n = 31$ and $P_\infty = 10582$ Pa.

### F. Effect of Freestream Static Pressure on the Mode Shape

The normalized radial, axial, and circumferential mode shapes for different values of $P_\infty$ are shown in Fig. 9. Here Eq. (20) is used to account for aerodynamic loading. When $P_\infty = 0.0$ Pa the eigenvectors are pure real and represent the free vibration of the shell in standing wave forms. For low values of freestream static pressure the eigenvectors are complex in regions where the imaginary part is close to zero and become negligible, but as $P_\infty$ increases each eigenvalue takes a complex mode shape, which can be represented by two real mode shapes. They are commonly called cosine and sine modes and are phase shifted by 90 deg. As a result, nodes and antinodes travel along the shell circumferentially and this means that the mode shapes contain traveling wave components. This behavior was also observed in the experiments [2]; the flutter motions were traveling wave forms with moving node lines.

### G. Effect of Shell Boundary Conditions

To establish the effects of shell boundary conditions on the critical freestream static pressures, some typical data are shown in Table 3. For the same shell geometry and flow parameters, the shell with one end free and the other end as simply supported loses its dynamic stability first. When both ends are free, flutter onset occurs with second- and third-mode coupling. For the other boundary conditions flutter onset starts by coalescence of the first and second longitudinal modes.

## VI. Conclusions

A hybrid finite element method in which the shape functions are found from the exact solution of Sander's shell theory resulted in a fast and efficient convergence to analyze the dynamic stability of circular cylindrical shells subjected to external supersonic flow.

The present approach has better agreement with existing experimental data than other analytical and FEM analyses for prediction of flutter onset. It is observed that piston theory with a curvature term provides a better approximation to account for fluid–structure interaction in supersonic airflow conditions. Numerical results are obtained for different shell boundary conditions and geometries. In all the study cases, only one type of instability is found, namely, coupled-mode flutter in the form of traveling wave flutter, mostly in the first and second longitudinal modes.

This proposed hybrid FEM provides the capability to apply different complex boundaries and geometries for a cylindrical shell. This can be used effectively in the design and analysis of aerospace structures. Reliable results can be obtained at less computational cost compared to commercial FEM software and analytical methods, which imposes some restrictions when such analysis is done.

Subsequent work to this study is presently being prepared to deal with the effect of geometry and aerodynamic nonlinearities on flutter boundaries. This should improve the reliability of the FEM package.

## Appendix A: Structural Equilibrium Equations

Sander's linear equation for thin cylindrical shells in terms of axial, tangential, and circumferential displacements is as follows [Eq. (4)]:

$$L_1(U,V,W,P_{ij}) = P_{11}\frac{\partial^2 U}{\partial x^2} + \frac{P_{12}}{R}\frac{\partial^2 U}{\partial x^2}\left(\frac{\partial^2 V}{\partial x\partial\theta} + \frac{\partial W}{\partial x}\right) - P_{14}\frac{\partial^3 W}{\partial x^3} + \frac{P_{15}}{R^2}\left(\frac{\partial^3 W}{\partial x\partial\theta^2} + \frac{\partial^2 V}{\partial x\partial\theta}\right) + \left(\frac{P_{33}}{R} - \frac{P_{63}}{2R^2}\right)\left(\frac{\partial^2 V}{\partial x\partial\theta} + \frac{1}{R}\frac{\partial^2 U}{\partial\theta^2}\right) + \left(\frac{P_{36}}{R^2} - \frac{P_{66}}{2R^3}\right)\left(-2\frac{\partial^3 W}{\partial x\partial\theta^2} + \frac{3}{2}\frac{\partial^2 V}{\partial x\partial\theta} - \frac{1}{2R}\frac{\partial^2 U}{\partial\theta^2}\right)$$

$$L_2(U,V,W,P_{ij}) = \left(\frac{P_{21}}{R} - \frac{P_{51}}{R^2}\right)\frac{\partial^2 U}{\partial x\partial\theta} + \frac{1}{R}\left(\frac{P_{22}}{R} + \frac{P_{52}}{R^2}\right) \times \left(\frac{\partial^2 V}{\partial\theta^2} + \frac{\partial W}{\partial\theta}\right) - \left(\frac{P_{24}}{R} + \frac{P_{54}}{R^2}\right)\frac{\partial^3 W}{\partial x^2\partial\theta} + \frac{1}{R^2}\left(\frac{P_{25}}{R} + \frac{P_{55}}{R^2}\right) \times \left(-\frac{\partial^3 W}{\partial\theta^3} + \frac{\partial^2 V}{\partial\theta^2}\right) + \left(P_{33} + \frac{3P_{63}}{2R}\right)\left(\frac{\partial^2 V}{\partial x^2} + \frac{\partial^2 U}{R\partial x\partial\theta}\right) + \frac{1}{R}\left(P_{36} + \frac{3P_{66}}{2R}\right)\left(-2\frac{\partial^3 W}{\partial x^2\partial\theta} + \frac{3}{2}\frac{\partial^2 V}{\partial x^2} - \frac{1}{2R}\frac{\partial^2 U}{\partial x\partial\theta}\right)$$

$$L_3(U,V,W,P_{ij}) = P_{41}\frac{\partial^3 U}{\partial x^3} + \frac{P_{42}}{R}\left(\frac{\partial^3 V}{\partial x^2\partial\theta} + \frac{\partial^2 W}{\partial x^2}\right) - P_{44}\frac{\partial^4 W}{\partial x^4} + \frac{P_{45}}{R^2}\left(-\frac{\partial^4 W}{\partial x^2\partial\theta^2} + \frac{\partial^3 V}{\partial x^2\partial\theta}\right) + \frac{2P_{63}}{R}\left(\frac{1}{R}\frac{\partial^3 U}{\partial x\partial\theta^2} + \frac{\partial^3 V}{\partial x^2\partial\theta}\right) + \frac{2P_{66}}{R^2}\left(-2\frac{\partial^4 W}{\partial x^2\partial\theta^2} + \frac{3}{2}\frac{\partial^3 V}{\partial x^2\partial\theta} - \frac{1}{2R}\frac{\partial^3 U}{\partial x\partial\theta^2}\right) + \frac{P_{51}}{R^2}\frac{\partial^3 U}{\partial x\partial\theta^2} + \frac{P_{52}}{R^3}\left(\frac{\partial^3 V}{\partial\theta^3} + \frac{\partial^2 W}{\partial\theta^2}\right) + \frac{P_{55}}{R^4}\left(-\frac{\partial^4 W}{\partial\theta^4} + \frac{\partial^3 V}{\partial\theta^3}\right) - \frac{P_{21}}{R}\frac{\partial U}{\partial x} - \frac{P_{54}}{R^2}\frac{\partial^4 W}{\partial x^2\partial\theta^2} + \frac{P_{22}}{R^2}\left(\frac{\partial V}{\partial\theta} + W\right) + \frac{P_{24}}{R^2}\frac{\partial^2 W}{\partial\theta^2} - \frac{P_{25}}{R^3}\left(-\frac{\partial^2 W}{\partial\theta^2} + \frac{\partial V}{\partial\theta}\right)$$

## Appendix B: Coefficient Matrices

### I. Shape Functions

Matrices $[T]_{3\times3}$, $[R]_{3\times8}$, and $[A]_{8\times8}$ are defined as

$$[T] = \begin{bmatrix} \cos(n\theta) & 0 & 0 \\ 0 & \cos(n\theta) & 0 \\ 0 & 0 & \sin(n\theta) \end{bmatrix} \qquad R(3,i) = \alpha_i e^{\lambda_i x/R}$$

$$R(2,i) = e^{\lambda_i x/R}, \qquad R(1,i) = \beta_i e^{\lambda_i x/R} \qquad i = 1,2,\ldots,8$$

$$A(1,i) = \alpha_i, \qquad A(2,i) = 1, \qquad A(3,i) = \frac{\lambda_i}{R}, \qquad A(4,i) = \beta_i$$

$$A(5,i) = \alpha_i e^{\lambda_i l/R} \qquad A(6,i) = e^{\lambda_i l/R}, \qquad A(7,i) = \frac{\lambda_i}{R}e^{\lambda_i l/R}$$

$$A(8,i) = \beta_i e^{\lambda_i l/R} \qquad i = 1,2,\ldots 8$$

### II. Strain Vector

The elements of matrix $[Q]$ of order $6 \times 8$ are given by

$$Q(1,i) = \alpha_i \frac{\lambda_i}{R} e^{\lambda_i x/R}, \qquad Q(2,i) = \frac{1}{R}(n\beta_i + 1)e^{\lambda_i x/R}$$

$$Q(3,i) = \frac{1}{R}(\beta_i \lambda_i - n\alpha_i)e^{\lambda_i x/R} \qquad Q(4,i) = -\left(\frac{\lambda_i}{R}\right)^2 e^{\lambda_i x/R}$$

$$Q(5,i) = \frac{1}{R^2}(n^2 + \beta_i n)e^{\lambda_i x/R}$$

$$Q(6,i) = \frac{1}{R^2}\left(2n\lambda_i + \frac{3}{2}\beta_i\lambda_i + \frac{1}{2}n\alpha_i\right)e^{\lambda_i x/R} \qquad i = 1, 2, \ldots 8$$

### III. Fluid Pressure Field

The elements of matrix $R_f$ of order $3 \times 8$ in Eq. (25) are

$$[R_f] = \begin{bmatrix} 0 & \ldots & 0 \\ e^{i(\lambda_1 x/R)} & \ldots & e^{i(\lambda_8 x/R)} \\ 0 & \ldots & 0 \end{bmatrix}$$

## Acknowledgments

The authors acknowledge the financial support of the Natural Sciences and Engineering Research Council of Canada, grant no. A8814.

## References

[1] Ashley, H., and Zartarian, G., "Piston Theory-New Aerodynamic Tool for Aeroelastician," *Journal of the Aeronautical Sciences*, Vol. 23, No. 12, 1956, pp. 1109–1118.

[2] Olson, M. D., and Fung, Y. C., "Supersonic Flutter of Circular Cylindrical Shells Subjected to Internal Pressure and Axial Compression," *AIAA Journal*, Vol. 4, No. 5, 1966, pp. 858–864. doi:10.2514/3.3558

[3] Olson, M. D., and Fung, Y. C., "Comparing Theory and Experiment for Supersonic Flutter of Circular Cylindrical Shells," *AIAA Journal*, Vol. 5, No. 10, 1967, pp. 1849–1856. doi:10.2514/3.4315

[4] Evensen, D. A., and Olson, M. D., "Nonlinear Flutter of a Circular Cylindrical Shell in Supersonic Flow," NASA TN D-4265, 1967.

[5] Evensen, D. A., and Olson, M. D., "Circumferentially Traveling Wave Flutter of Circular Cylindrical Shell," *AIAA Journal*, Vol. 6, No. 8, 1968, pp. 1522–1527. doi:10.2514/3.4799

[6] Horn, W., Barr, G., Carter, L., and Stearman, R., "Recent Contributions to Experiments on Cylindrical Shell Panel Flutter," *AIAA Journal*, Vol. 12, No. 11, 1974, pp. 1481–1490. doi:10.2514/3.49533

[7] Dowell, E. H., "Flutter of Infinitely Long Plates and Shells. Part II," *AIAA Journal*, Vol. 4, No. 9, 1966, pp. 1510–1518. doi:10.2514/3.3728

[8] Dowell, E. H., *Aeroelasticity of Plates and Shells*, Noordhoff International, Leyden, The Netherlands, 1975.

[9] Carter, L. L., and Stearman, R. O., "Some Aspects of Cylindrical Shell Panel Flutter," *AIAA Journal*, Vol. 6, No. 1, 1968, pp. 37–43. doi:10.2514/3.4438

[10] Barr, G. W., and Stearman, R. O., "Aeroelastic Stability Characteristics of Cylindrical Shells Considering Imperfections and Edge Constraint," *AIAA Journal*, Vol. 7, No. 5, 1969, pp. 912–919. doi:10.2514/3.5244

[11] Barr, G. W., and Stearman, R. O., "Influence of a Supersonic Flow Field on The Elastic Stability Of Cylindrical Shells," *AIAA Journal*, Vol. 8, No. 6, 1970, pp. 993–1000. doi:10.2514/3.5821

[12] Amabili, M., and Pellicano, F., "Nonlinear Supersonic Flutter of Circular Cylindrical Shells," *AIAA Journal*, Vol. 39, No. 4, 2001, pp. 564–573. doi:10.2514/2.1365

[13] Amabili, M., and Pellicano, F., "Multimode Approach to Nonlinear Supersonic Flutter of Imperfect Circular Cylindrical Shells," *Journal of Applied Mechanics*, Vol. 69, No. 2, 2002, pp. 117–129. doi:10.1115/1.1435366

[14] Bismarck-Nasr, M. N., "Finite Element Method Applied to The Supersonic Flutter of Circular Cylindrical Shells," *International Journal for Numerical Methods in Engineering*, Vol. 10, No. 2, 1976, pp. 423–435. doi:10.1002/nme.1620100212

[15] Ganapathi, M., Varadan, T. K., and Jijen, J., "Field-Consistent Element Applied to Flutter Analysis of Circular Cylindrical Shells," *Journal of Sound and Vibration*, Vol. 171, No. 4, 1994, pp. 509–527. doi:10.1006/jsvi.1994.1137

[16] Bismarck-Nasr, M. N., "Finite Elements in Aeroelasticity of Plates and Shells," *Applied Mechanics Reviews*, Vol. 49, No. 10S, 1996, pp. S17–S24. doi:10.1115/1.3101970

[17] Lakis, A. A., and Paidoussis, M. P., "Dynamic Analysis of Axially Non-Uniform Thin Cylindrical Shells," *Journal of Mechanical Engineering Science*, Vol. 14, No. 1, 1972, pp. 49–71. doi:10.1243/JMES_JOUR_1972_014_009_02

[18] Sabri, F., and Lakis, A. A., "Hydroelastic Vibration of Partially Liquid-Filled Circular Cylindrical Shells Under Combined Internal Pressure and Axial Compression," AIAA Paper 2009-2646, May 2009.

[19] Krumhaar, H., "The Accuracy of Linear Piston Theory When Applied to Cylindrical Shells," *AIAA Journal*, Vol. 1, No. 6, 1963, pp. 1448–1449. doi:10.2514/3.1832

[20] Sanders, J. L., "An Improved First-Approximation Theory for Thin Shell," NASA R-24, 1959.

[21] Toorani, M. H., and Lakis, A. A., "General Equations of Anisotropic Plates and Shells Including Transverse Shear Deformations, Rotary Inertia and Initial Curvature Effects," *Journal of Sound and Vibration*, Vol. 237, No. 4, 2000, pp. 561–615. doi:10.1006/jsvi.2000.3073

[22] Zienkiewicz, O. C., and Taylor, R. L., *The Finite Element Method: Volume 2, Solid Mechanics*, Butterworht–Heinemann: Oxford, 2000.

[23] MacNeal, R. H., "Nastran Theoretical Manual," NASA SP-221, 1972.

E. Livne
*Associate Editor*